Original Article | Journal of Biosystems Engineering

J. of Biosystems Eng. 39(2):142-149. (2014. 6)
http://dx.doi.org/10.5307/JBE.2014.39.2.142

eISSN : 2234-1862
pISSN : 1738-1266

A Simple Multispectral Imaging Algorithm for Detection of Defects on Red Delicious Apples

Hoyoung Lee[1], Chun-Chieh Yang[1], Moon S. Kim[1]*, Jongguk Lim[2], Byoung-Kwan Cho[3], Alan Lefcourt[1], Kuanglin Chao[1], Colm D. Everard[4]

[1]Environmental Microbial and Food Safety Laboratory, Beltsville Agricultural Research Center, Agricultural Research Service, United States Department of Agriculture, 10300 Baltimore Ave, Beltsville, MD 20705
[2]National Academy of Agricultural Science, Rural Development Administration, Suwon 441-100, Republic of Korea
[3]Department of Biosystems Machinery Engineering, Chungnam National University, Daejeon, 305-764, Republic of Korea
[4]School of Biosystems Engineering, University College Dublin, Dublin 4, Ireland

Received: April 25th 2014; Revised: May 26th 2014; Accepted: June 1st 2014

Abstract

Purpose: A multispectral algorithm for detection and differentiation of defective (defects on apple skin) and normal Red Delicious apples was developed from analysis of a series of hyperspectral line-scan images. **Methods:** A fast line-scan hyperspectral imaging system mounted on a conventional apple sorting machine was used to capture hyperspectral images of apples moving approximately 4 apples per second on a conveyor belt. The detection algorithm included an apple segmentation method and a threshold function, and was developed using three wavebands at 676 nm, 714 nm and 779 nm. The algorithm was executed on line-by-line image analysis, simulating online real-time line-scan imaging inspection during fruit processing. **Results:** The rapid multispectral algorithm detected over 95% of defective apples and 91% of normal apples investigated. **Conclusions:** The multispectral defect detection algorithm can potentially be used in commercial apple processing lines.

Keywords: Apples, Defect detection, Hyperspectral imaging, Line-scan imaging, Multispectral

Introduction

The U.S. produces 7% of the total world apple production—over 4 million metric tons annually (USDA, 2005). Among the many apple varieties in the U.S., the Red Delicious is the top variety planted and produced (Slattery et al., 2011). According to U.S. guidelines for apple sales, defective apples should not exceed 10% of the apples in any lot, no more than 5% of the apples in the lot should be seriously damaged, and less than 1% of the apples in the lot should be affected by decay or internal breakdown (USDA, 2002). However, even with such a low tolerance, defective apples still present potential for causing foodborne illness. A variety of cases of foodborne illness related to contaminated fruits were reported in the U.S. during the past decade (FDA, 2001, 2006). Automatic online detection of defective apples could help the industry to increase efficiency and reduce food safety risks.

Several recent research studies have been carried out to develop image-processing methods for the detection of defective apples (Bhatt et al., 2012; Garrido-Novell et al., 2012; Kim et al., 2007; Srivastava, 2012; Unay et al., 2011). Using processing and analysis methods for full-target images, these studies found that effective algorithms could be developed for non-destructive detection of defective apples using a variety of machine vision systems. With a high-speed camera and an appropriate imaging spectrograph, a line-scan-based machine vision system can continuously acquire a series of line-scan images

***Corresponding author:** Moon S. Kim
Tel: +1-301-504-8450; **Fax:** +1-301-504-9466
E-mail: moon.kim@ars.usda.gov

with full-spectrum data at each pixel on the line-scans. Hyperspectral image analysis can be used to select specific essential wavebands relevant to the targeted inspection task from among hundreds of available wavebands (Kim et al., 2001, 2002; Mehl et al., 2002). Further multispectral data analysis based on those wavebands can be used to develop a multispectral function specifically for line-by-line image analysis for the targeted inspection task, as opposed to full-target image analysis applied after accumulating a "complete set" of line scans for each target item. The line-scan-based multispectral inspection function can then be implemented on a high-speed commercial food processing line by a line-scan machine vision system (Kim et al., 2008; Yang et al., 2010) more easily than a full-target imaging analysis method, given fewer concerns regarding sequential target separation and accommodation for variations in sample size or processing line speeds.

The objective of this study is the development of a simple, line-scan-based multispectral algorithm to detect defects on Red Delicious apples and separate them from normal ones. Guidelines for algorithm development included selection of a small number of wavebands, to support rapid data transfer and high-speed computation in a future real-world application, and more importantly, line-by-line image processing and analysis methods to ensure suitability for online line-scan inspection for high-speed apple processing operations.

Materials and Methods

Apple collection

Red Delicious apples were obtained from the Rice Fruit Company (Gardners, PA), collected randomly from lots of "tree-run" apples to which no wax or other coating was applied after harvest, and classified visually. Apples visually meeting with the requirements of the grades of U.S. Extra Fancy, U.S. Fancy, U.S. No. 1, and U.S. No. 1 Hail were classified as normal apples. Apples with clear injuries, damages by insects, internal breakdowns, or decays were classified as defective apples. The apples were transported to the Environmental Microbiological and Food Safety Laboratory (EMFSL)at Beltsville, MD, and stored in a 4°C cold room prior to scanning. This study used a total of 183 Red Delicious apples—98 normal and 85 defective apples.

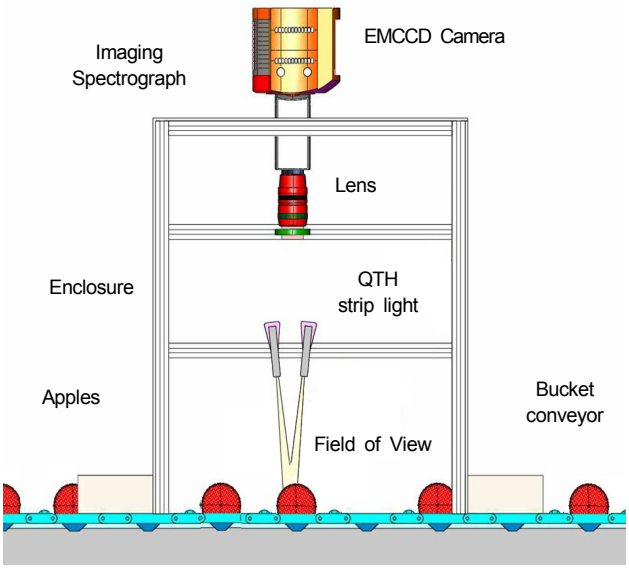

Figure 1. The general experimental design and major components of the hyperspectral line-scan imaging system.

Hyperspectral line-scan imaging system

The sensing component of the hyperspectral line-scan machine vision system used in this research consisted of an iXon DU-860 electron-multiplying-charge-coupled-device (EMCCD) camera (Andor Technology PLC, Belfast, Northern Ireland), an ImSpector V8E imaging spectrograph (Specim, Oulu, Finland), and a Schneider-Kreuznach Xenoplan 1.4/35 C-mount lens (Schneider Optics, Hauppauge, NY). Light from a pair of 150-watt quartz-tungsten halogen (QTH) lamps was channeled through fiber-optic line-light assemblies to provide illumination to the linear field of view (FOV). The machine vision system was installed to view apples in the conveyor lane of a commercial-type apple sorting machine (FMC Corp, Philadelphia, PA). The sensing and illumination components were mounted within a black enclosure to eliminate the effects of ambient light. To simplify image analysis, the apple-holding cups of the sorting machine were painted black for easy target segregation. Figure 1 shows a schematic of the of the line-scan machine vision system on the apple conveyor. For a detailed description of the imaging system, readers are referred to an article by Kim et al. (2008).

Line-scan image acquisition

For image acquisition, the apples were dumped into the loading end of the apple sorter so as to randomize the orientation of the apples in the conveyor cups as viewed by the overhead camera. The conveyor cups moved the

apples across the camera's FOV at approximately 4 apples per second as the machine vision system acquired a series of line-scan images. Each line-scan image included spectral data along one axis and spatial data along another axis. The EMCCD camera produced hyperspectral images sized 128 (spatial) × 128 (spectral). The size was reduced by binning the spectral dimension by two in the buffer of the camera, before transferring the data to the computer, to output line-scans sized 128 (spatial) × 64 (spectral). The spectrum for each pixel spanned 535 nm to 831 nm across 64 (approx. 4.7 nm intervals) wavebands. Multiple series of line-scans were acquired to form hyperspectral images used for image analysis and algorithm development. These hyperspectral images contained sequences of either 9 to 10 normal apples or 5 defective apples, with approximately 80 to 90 line-scans required to complete the scan of the top-facing side of one apple (not including the spaces between apples). Therefore, individual apple scene consisted of approximately 85 x 128 pixels.

Each line-scan was calibrated using a reference white and dark line-scan. For the white reference, a white 99% diffuse reflectance target (Spectralon, Labsphere, North Sutton, NH) was placed on the conveyor of the sorting machine and 38 line-scans of the target were acquired. The 38 line scans were averaged to create the reference white, W. Next, the QTH lights were turned off and the camera lens was covered for the acquisition of 26 dark-current line scans, which were then averaged to create the reference dark, D. The numbers of line images for both references were set arbitrarily. The references W and D were used to convert raw reflectance images I_0 of apples to relative reflectance images I, according to the following Equation (1):

$$I = \frac{I_0 - D}{W - D} \quad (1)$$

Hyperspectral image analysis

Images of ten normal and five defective apples were randomly selected to create a sample group from all the hyperspectral images acquired. The images of the other 88 normal and 80 defective apples were used as a test group. The sample group was used for spectral analysis, waveband selection, and development of threshold function and a multispectral line-scan-based inspection algorithm. The inspection algorithm was then applied to the test group for algorithm validation.

From the sample group images, sample pixels belonging to each of six pixel categories were visually identified: (1) 243 "defect" pixels where clear damage or decay was observed on defective apples; (2) 2601 "defect_N" pixels on damage-free apple-skin areas of defective apples; (3) 45 "defect_S" pixels on the stems of defective apples; (4) 4410 "normal" pixels on apple-skin areas of normal apples; (5) 117 "normal_S" pixels on the stems of normal apples; and (6) 2299 "background" pixels located outside the perimeter of the apples but within the area of the hyperspectral images. The average spectra calculated from these sample pixels for the six categories are shown in Figure 2.

Except for the background spectrum, each of the other five average pixel spectra showed three broad peaks. For the spectral range between 535 nm and 676 nm, although the curves of the five average spectra seemed to be clearly different from one another, the variations shown by individual pixel spectra were large enough to consider the intensity differences significant. For the spectral range between 779 nm and 831 nm, it was difficult to observe any difference among the curves of the average spectra except for the magnitude of the relative intensity in each spectrum. However, the magnitude of the relative intensity can be significantly affected by variations of sample shapes and sizes. In the spectral range between 676 nm and 779 nm in Figure 2, all five apple-pixel categories show a maximum relative intensity in their average spectra between 709 nm and 718 nm. Thus, the wavelength at the center of this narrow range, 714 nm, was selected. These average spectra also showed local minima values at either 676 nm or 779 nm. Comparing the spectra in Figure 2, the intensity difference between 714 nm and 676 nm for the normal category was obviously lower than that for the other four apple-pixel categories. Such a difference was also observed between 714 nm and 779 nm. Therefore, the three wavelengths of 676 nm, 714 nm, and 779 nm were selected for the algorithm development.

Moreover, the relative intensity for the average background spectrum was higher at 676 nm than at 714, unlike all the average apple-pixel spectra. Also, the relative intensity at 779 nm for the background was much lower than that for any other category. Although the magnitude of the relative intensity was not to be used for defective apple detection, it could be appropriately used

for segmentation of apples from the image background. These observations further suggested that development of the defective apple detection algorithm could succeed using only the three wavelengths of 676 nm, 714 nm, and 779 nm.

Apple segmentation method

Two ratios were calculated as follows, using relative intensity values at the three selected key wavebands, 676 nm, 714 nm, and 779 nm, to characterize the spectral difference between 676 nm and 779 nm in Figure 2,

$$R_{676/714} = \frac{I_{676}}{I_{714}} \tag{2}$$

$$R_{779/714} = \frac{I_{779}}{I_{714}} \tag{3}$$

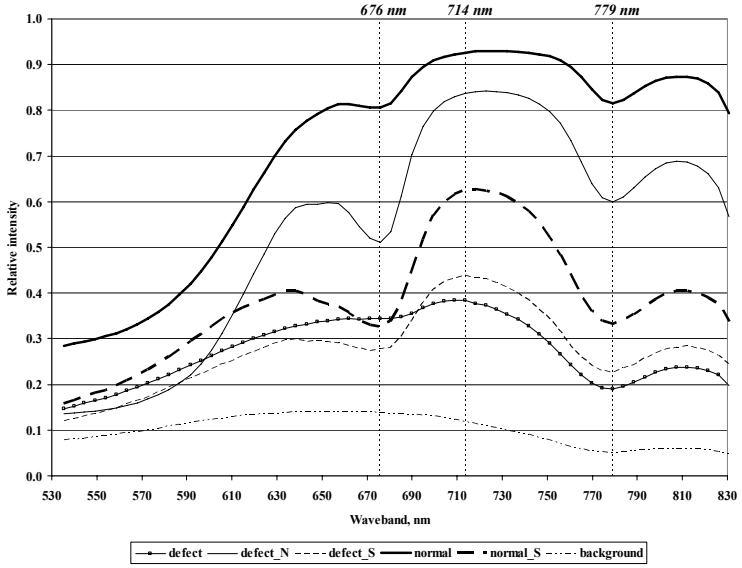

Figure 2. The average spectra for the categories of (1) defect, where clear damages or decays were observed in defect apples; (2) defect_N, where no clear damages were observed in defect apples; (3) defect_S, where was stem in defect apples; (4) normal, where was apple skins in normal apples; (5) normal_S, where was stem in normal apples; and (6) background, where there was no apple at all.

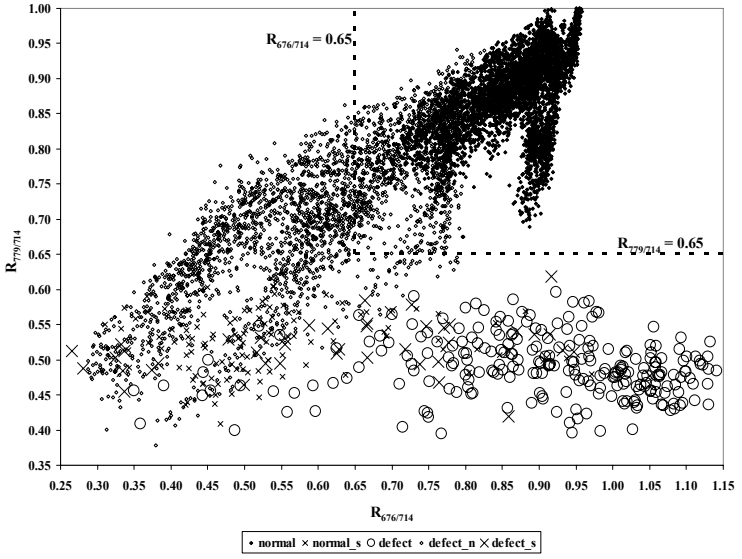

Figure 3. The ratios of relative intensities for the apple pixels from the sample group of apples.

where I_{676}, I_{714}, and I_{779} are the relative intensities at 676 nm, 714 nm, and 779 nm, respectively. Both ratio functions were applied to all the sample group pixels in the categories of "normal", "normal_S", "defect", "defect_N", and "defect_S". The results are shown in Figure 3. For the 4410 pixels of the normal pixel category (normal apple skin on normal apples), both ratio values were always higher than 0.65. Figure 3 shows that only part of 2601 pixels of the "defect_N" category (normal apple skin on defect apples) contained both ratio values higher than 0.65. Therefore, any pixel with two ratio values above 0.65 was identified as a normal apple pixel, while any pixel with a value below 0.65 for either $R_{676/714}$ or $R_{779/714}$ was identified as a suspected defective apple pixel.

The $R_{676/714}$ ratio function was also used to segment apples from image background areas. A pixel was considered as part of an apple only when the value of $R_{676/714}$ was lower than or equal to 1.0. However, the preliminary study also showed that scattered false-positive pixels could occur in the background areas as noise. The I_{779} relative intensities at these noise pixels were much lower than ones at the apple pixels. Based on the empirical evidence, any pixel was considered to be part of an apple only if it also had an I_{779} value higher than or equal to 0.18. Figure 4 shows images at 714 nm for normal and defective apples from the sample group and the segementation masks created using the $R_{676/714}$ ratio function and I_{779} criteria.

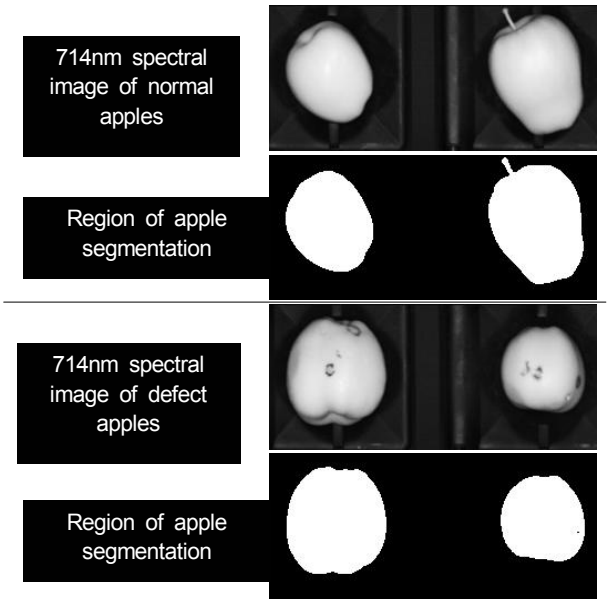

Figure 4. Example images of normal and defect Red Delicious apples at 714 nm and binary images after apple segmentation.

Feature values of an apple

To simulate real-time line-scanning of apples, each line was retrieved in sequence from the hyperspectral apple images for line-by-line analysis. When no pixel in a line was identified as part of an apple, this image was discarded and the next line image was retrieved. This process was repeated until one or more pixels in the scanned line was identified as part of an apple, at which time each of the ratio functions, $R_{676/714}$ and $R_{779/714}$ were applied. Each pixel was assigned a value of 1 if its $R_{676/714}$ value was greater than the 0.65 threshold value (normal pixel), or a value of 0 if otherwise (suspected defective apple pixel). Likewise, each pixel was also assigned a second value of 1 or 0 based on its $R_{779/714}$ value. Thus, each pixel within the apple area would be given two binary values resulting from $R_{676/714}$ and $R_{779/714}$. This process was repeated for every line image up until a line image was retrieved that contained no pixels identified as part of an apple, thereby indicating completion of one apple scan. For the set of all line scans for that one apple, the average of all the apple pixels' binary values assigned from $R_{676/714}$ was then calculated as $AR_{676/714}$ for the apple. Similarly, the average of all the pixels' binary values assigned from $R_{779/714}$, $AR_{779/714}$, was calculated for the apple. In this way, two spectral feature values, $AR_{676/714}$ and $AR_{779/714}$, were obtained for each apple.

Threshold function development

Two feature values, $AR_{676/714}$ and $AR_{779/714}$, were calculated for each of the ten normal and five defective apples in the sample group and are plotted in Figure 5. The result shows two data clusters corresponding to the normal subgroup and defective subgroup. The center point (momentum) of each cluster was determined by calculating the average $AR_{676/714}$ and $AR_{779/714}$ values for each subgroup. The line connecting the two center points was then calculated:

$$AR_{779/714} = 0.212 \times AR_{676/714} + 0.3386 \quad (4)$$

To separate the two clusters, a mirror line of the connection line (momentum) in Equation (4), intersecting through the center of the connection line at the mirror point in Figure 5, was calculated as follows:

$$AR_{779/714} = -0.212 \times AR_{676/714} + 0.5549 \quad (5)$$

Equation (5) was used as the threshold function to detect defective Red Delicious apples and separate them from normal ones. A threshold function used $AR_{676/714}$ and $AR_{779/714}$ from the sample set in that for a normal apple, the left side of the function is greater than or equal to the right side of the function. If the left side of the function is less than the right side, the apple is defective. This algorithm, including the apple segmentation method, the feature values calculation, and the threshold function, was applied to all the apple images in the test group for validation.

Results and Discussion

Although two of 10 normal apples in the sample group were incorrectly identified as defective apples, as seen in Figure 5, the identification result for the test group apples was better than that for the sample group. Figure 6 shows the result for evaluation of the defective apple detection algorithm on the test group of 88 normal and 80 defective Red Delicious apples. Approximately 91% of normal apples (80 of 88) and 95% of defective apples (76 of 80) were successfully identified by the threshold function.

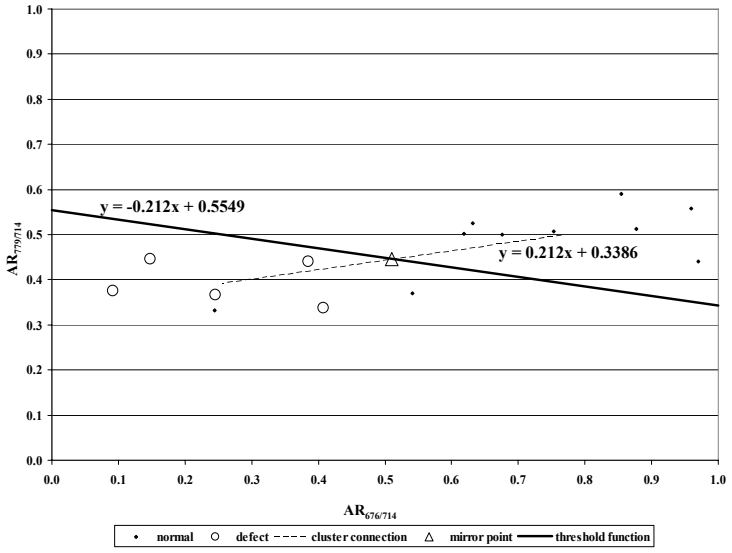

Figure 5. The development of the threshold equation, y=-0.212x+0.5549, using five defect and 10 normal Red Delicious apples in the sample group.

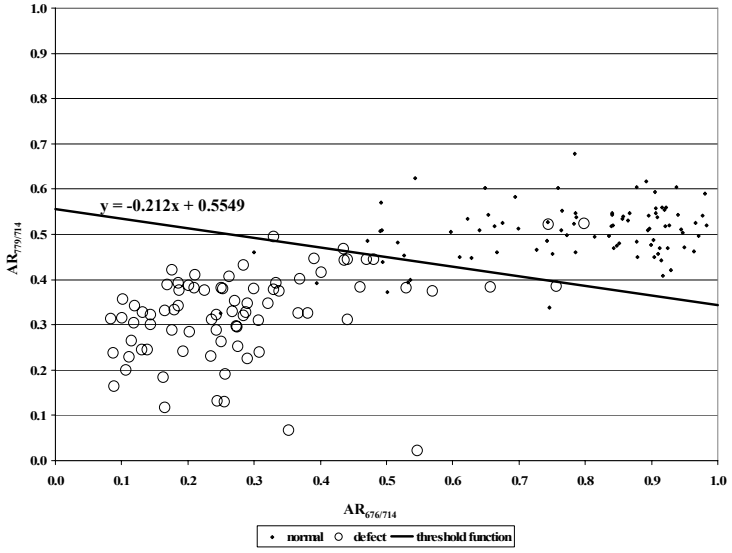

Figure 6. Test group result for separation of 80 defect apples from 88 normal apples using the threshold equation.

The algorithm spent less than 0.03 seconds to complete the processing of the line scans for each apple and to obtain the identification result. The algorithm was executed by MATLAB R2011b (MathWorks, Inc., Natick, MA) run on a PC with an Intel Core™2 Duo E8500 processor at 3.16 GHz and Microsoft Windows XP. This identification performance and fast computation speed show that the algorithm has potential to be applied to commercial processing lines and to meet the current requirement by the USDA for defective apples to not exceeding 10% of all apples in any one lot.

To further investigate the results shown in Figures 5 and 6, each incorrectly identified apple image was carefully compared visually with other correctly identified images. For the ten normal apples identified as defective apples in the sample and test groups, the stem end areas around the fruits' stems tended to be much darker at either 676 nm or 779 nm than other normal areas, and the numbers of pixels in these darker areas were high. One normal apple was incorrectly identified because its calyx or bottom was identified as a large suspected crack. Also, the overall size of some of these apples was much smaller than many of the other normal apples. In this condition, pixels around the periphery of an apple tended to be darker at either 676 nm or 779 nm, and the smaller apple area allowed these suspect pixels to account for a larger fraction of the total number of pixels than was typical for other normal apples. Thus, these pixels in these areas were incorrectly determined as defect pixels and the whole apples were thus identified as defective apples.

Figure 5 shows that, unlike the normal apples, all five defective apples in the sample group were correctly identified. For the test group in Figure 6, four defective apples were incorrectly identified as normal ones. Compared with other correctly identified defective apples, these had either only a few small cracks or were gently bruised but with relatively healthy skins. They were also larger than most of the other defective apples, which made the portion of suspected defect area account for a much smaller fraction of the total imaged area of the whole apple. These misidentifications were for fruit conditions that might contribute to lower apple quality without necessarily causing a food safety problem.

To overcome these challenges, future testing might use an improved light source for better illumination. In this research, two QTH lamps were used, but the illumination may not have been ideal for line-scanning of curved objects such as apples. For the misidentified normal apples, when the calyx or the apple bottom was shown in the image and the surrounding area was poorly illuminated, the shadow in this area might be confused with being a real defect. Moreover, the peripheral areas of the fruit were usually misidentified as suspected defects due to the current illumination regime.

In contrast, for the incorrectly identified defective apples, when the defects were small cracks or bumps and were over-illuminated, the defects could be easily ignored by the imaging system. The result in Figure 6 indicated that the relatively large apples with small cracks (defects) could be easily misidentified as normal ones. A better illumination design, such as more diffused light, could be included in future development and improvement of the line-scan system for apple inspection. Another improvement to be investigated for future development is to rotate the apple in place in front of the camera so that the whole apple body could be scanned.

Using the apple segemetation method, the multispectral algorithm based on the hyperspectral image data at 676 nm, 714 nm and 779 nm quickly and correctly detected each individual apple. Rapid calculations by the threshold function based on two relative intensity ratios, between 676 nm and 714 nm, and between 779 nm and 714 nm, means the algorithm is well suited to real-time online use in a processing line. The line-scan machine vision system could be easily installed on existing processing lines, and the algorithm to detect defective apples would help the apple industry to ensure food safety and quality.

Conclusions

A hyperspectral line-scan imaging system consisting of an EMCCD camera, spectrograph, and lens was used to acquiring images of 98 normal and 85 defective Red Delicious apples on a conveyor in a commercial apple sorting machine. From the hyperspectral image analysis, a simple multispectral algorithm was developed to detect the defective apples and differentiate them from the normal ones. Three key wavebands, 676 nm, 714 nm, and 779 nm, were selected, and an apple segmentation method and a threshold function were developed using the multispectral image data at these three wavebands. Two ratios of the relative intensities, $R_{676/714}$ and $R_{779/714}$, were used to calculate the threshold function for the

multispectral defective apple detection algorithm. The algorithm successfully detected 95% of 80 defective apples and 91% of 88 normal apples in a test group. The algorithm could complete scanning and obtain the detection result for an apple in less than 0.03 seconds. The detection performance of the algorithm shows its potential for use with high-speed nondestructive machine vision systems to help ensure food safety and quality, increase efficiency, and reduce costs for the apple industry.

Conflict of Interest

No potential conflict of interest relevant to this article was reported.

Acknowledgement

This study was carried out with the partial support of "Research Program for Agricultural Science & Technology Development (Project No. PJ009399)", National Academy of Agricultural Science, Rural Development Administration, Republic of Korea, and High Value-added Food Technology Development Program, Ministry of Agriculture, Food and Rural Affairs(MAFRA), Republic of Korea.

References

Bhatt, A. K., Pant, D and R. Singh. 2012. An analysis of the performance of artificial neural network techniques for apple classification: Open Forum, May 2012: AI & Society.

FDA. 2006. Questions & Answers: Taco Bell E. 2006. E. coli O157:H7 lettuce outbreak. Washington, DC.: Food and Drug Administration.

FDA. 2001. Hazard analysis and critical control point (HAACP); procedures for the safe and sanitary processing and importing of juices. Washington, DC.: Food and Drug Administration.

Garrido-Novell, C., Perez-Marin, D., Amigo, J. M., Fernandez-Novales, J., Guerrero, J. E and A. Garrido-Varo. 2012. Grading and color evolution of apples using RGB and hyperspectral imaging vision cameras. Journal of Food Engineering 113(2):281-288.

Kim, M. S., Chen, Y. R and P. M. Mehl. 2001. Hyperspectral reflectance and fluorescence imaging system for food quality and safety. Trans. ASAE 44(3):721-729.

Kim, M. S., Lefcourt, A. M., Chao, K., Chen, Y. R and I. Kim. 2002. Multispectral detection of fecal contamination on apples based on hyperspectral imagery - Part I: Application of visible-Near Infrared reflectance imaging. Trans. ASAE 45(6):2027-2037.

Kim, M. S., Chen, Y. R., Cho, B., Lefcourt, A. M., Chao, K and C. C. Yang. 2007. Hyperspectral reflectance and fluorescence line-scan imaging for online quality and safety inspection of apples. Sensing and Instrumentation for Food Quality and Safety 1(3):151-159.

Kim, M. S., Lee, K., Chao, K., Lefcourt, A. M., Jun, W. and D. E. Chan. 2008. Multispectral line-scan imaging system for simultaneous fluorescence and reflectance measurements of apples. Sensing and Instrumentation for Food Quality and Safety 2(2):123-129.

Mehl, P. M., Chao, K., Kim, M. S and Y. R. Chen. 2002. Detection of contamination on selected apple cultivars using hyperspectral and multispectral image analysis. Appl. Eng. of Agri. 18(2):219-226.

Slattery, E., Livingston, M., Greene, C and K. Klonsky. 2011. Characteristics of conventional and organic apple production in the United States. Report FTS-347-01. Washington, DC.: Economic Research Service, United States Department of Agriculture.

Srivastava, D. K. 2012. Efficient fruit defect detection and Glare removal algorithm by anisotropic diffusion and 2D Gabor filter. International Journal of Engineering Science & Advanced Technology 2(2):352-357.

Unay, D., Gosselin, B., Kleynen, O., Leemans, V., Destain, M. F and O. Debeir. 2011. Automatic grading of bi-colored apples by multispectral machine vision. Computers and Electronics in Agriculture 75(1):204-212.

USDA. 2005. U.S. Fruit and Vegetable Availability and Handling Charts. Washington, DC.: United States Department of Agriculture.

USDA. 2002. United States Standards for Grades of Apples. Washington, DC.: United States Department of Agriculture.

Yang, C. C., Kim, M. S., Kang, S., Cho, B. K., Chao, K., Lefcourt, A. M and D. E. Chan. 2012. Red to far-red multispectral fluorescence image fusion for detection of fecal contamination on apples. Journal of Food Engineering 108(2):312-319.